Mineralogia, vol. 56, 2025, 94-102 *Letter*

DOI: 10.2478/mipo-2025-0010

New occurrence of magnesites in Prins Karls Forland, Svalbard

Grzegorz Ziemniak[1,*], Maciej Manecki[2], Laura Lis[2]

[1]Institute of Geological Sciences, University of Wrocław, Pl. M. Borna 9, 50-204 Wrocław, Poland

[2]AGH University of Krakow, Faculty of Geology, Geophysics and Environmental Protection, 30 Mickiewicza Av., 30-059 Kraków, Poland

*Corresponding author: grzegorz.ziemniak@uwr.edu.pl

Abstract

This study reports the discovery of a large occurrence of magnesite metacarbonates above the northern shore of Selvågen, Prins Karls Forland (PKF), Svalbard. The stratabound magnesite occurs within the Scotiafjellet Group metasedimentary rocks of PKF and represents the first documented example of a magnesite in this region of Svalbard. The magnesite is hosted by cryptocrystalline metacarbonates containing distinctive chert bands and nodules, with associated mineral assemblages including quartz, dolomite, albite, muscovite, and pyrite. Petrographic features, such as zoned magnesite with Fe-rich rims and foliated carbonate matrices, suggest multiphase formation under greenschist facies conditions. Raman spectroscopy of carbonaceous material indicates metamorphic temperatures of 260–360°C. The magnesite likely formed through fluid-mediated metasomatism during Caledonian tectonism, with magnesium-rich fluids potentially sourced from devolatilized ultramafic complexes. This discovery enhances understanding of Svalbard's tectonometamorphic evolution and suggests that PKF may hold broader geological and paleobiological significance, especially given the presence of organic-rich cherts containing bioclasts.

Keywords: Regional geology of Svalbard, Raman geothermometry, Metacarbonates, Metacherts, Microfossils in cherts

1. Introduction

Magnesites are rocks that commonly form in the stratabound sedimentary environment or that are associated with alteration processes of ultramafic rocks (Schroll, 2002). From petrological point of view formation of magnesites can be related to precipitation due to evaporation at Earth's surface, but most often requires either chemical weathering or hydrothermal alteration of primary carbonate or ultramafic rock (Scheller et al., 2021). The involvement of hydrothermal fluids that carbonated ultramafic rocks and, after migrating toward the Earth's surface, precipitated magnesite deposits has been proposed for several occurrences (e.g., Yu et al., 2024; Zedef et al., 2000). For deeper magnesite deposits, the provenance of the fluids responsible for magnesitization remains a subject of ongoing debate.

To date, magnesite occurrences in Svalbard are strictly connected to the high-pressure (HP) rocks cropping out along Oscar II Land coast and mark subduction event in the Ordovician (Bernard-Griffiths et al., 1993; Ohta et al., 1995). Magnesite is hosted by green-brown dolostone and its association with serpentinites and presence of chromium minerals such as chromite and fuchsite unequivocally suggest its origin as resulting from hydrothermal alteration of ultramafic rocks (Ohta et al., 1995).

Here we describe a newly discovered occurrence of magnesites, tentatively interpreted as a stratabound deposit of possibly the Veitsch-type in Prins Karls Forland (PKF), Svalbard confirmed using optical and X-ray diffraction methods. A geothermometer based on Raman spectra of carbonaceous matter (Kouketsu et al., 2014) provided formation temperatures in the range of 260–360°C. We hypothesize that magnesites were reform at the lower greenschist-facies metamorphic conditions during tectonic assembly of western Svalbard as a result of metasomatism aided by fluids originating from hydrothermal alteration of neighbouring ultramafic rocks.

2. Samples and Methods

2.1. Geological background

PKF is a westernmost island in the Svalbard Archipelago (Fig. 1A). It is a part of the Southwestern Basement Province in the traditional tripartite division of Svalbard's crystalline basement (Gee & Teben'kov, 2004). This province is characterized by occurrences of the Torellian metamorphism, the early Caledonian HP metamorphic rocks as well as Ellesmerian metamorphic rocks (Majka & Kośmińska, 2017) and is divided into several terranes including the Prins Karls Terrane that encompasses the PKF (Wala et al., 2021).

The island is built of two parts, northern and southern, that are juxtaposed on the N-S trending Baklia Shear Zone that runs from Selvågen to Haukebukta (Hjelle et al., 1979); (Fig. 1B). The southern part of the island is composed of Neoproterozoic metasedimentary succession intercalated with minor volcanics and occurs only locally in the northern part of the island where it overthrusts the northern successions (e.g. Manby, 1986). The northern part consists predominantly of the carbonate and siliciclastic dominated Grampian Group that is underlain by the Scotiafjellet Group comprising phyllites, slates and metacarbonates with chert nodules (Hjelle et al., 1979; Tyrrell, 1924). These two groups of preassumably late Neoproterozoic age locally overthrust the Pinkie Group which is a Neoproterozoic complex metamorphosed under amphibolite facies conditions during the Ellesmerian Orogeny (Kośmińska et al., 2020). PKF was subjected to at least three tectonic events including Caledonian, Ellesmerian and Eurekan episodes. The earliest deformation and metamorphism was connected to westward folding and thrusting, and subsequent rejuvenation of tectonic structures (Manby, 1986; Schneider et al., 2019). In the northern PKF tectonic discontinuities are accompanied by carbonate veins composed of siderite, dolomite and pyrite.

Dark grey magnesite rock weathering to olive-green, forms a hill which clearly stands out on the northern shore of Selvågen NW above the ruins of the cottage (Fig. 2;

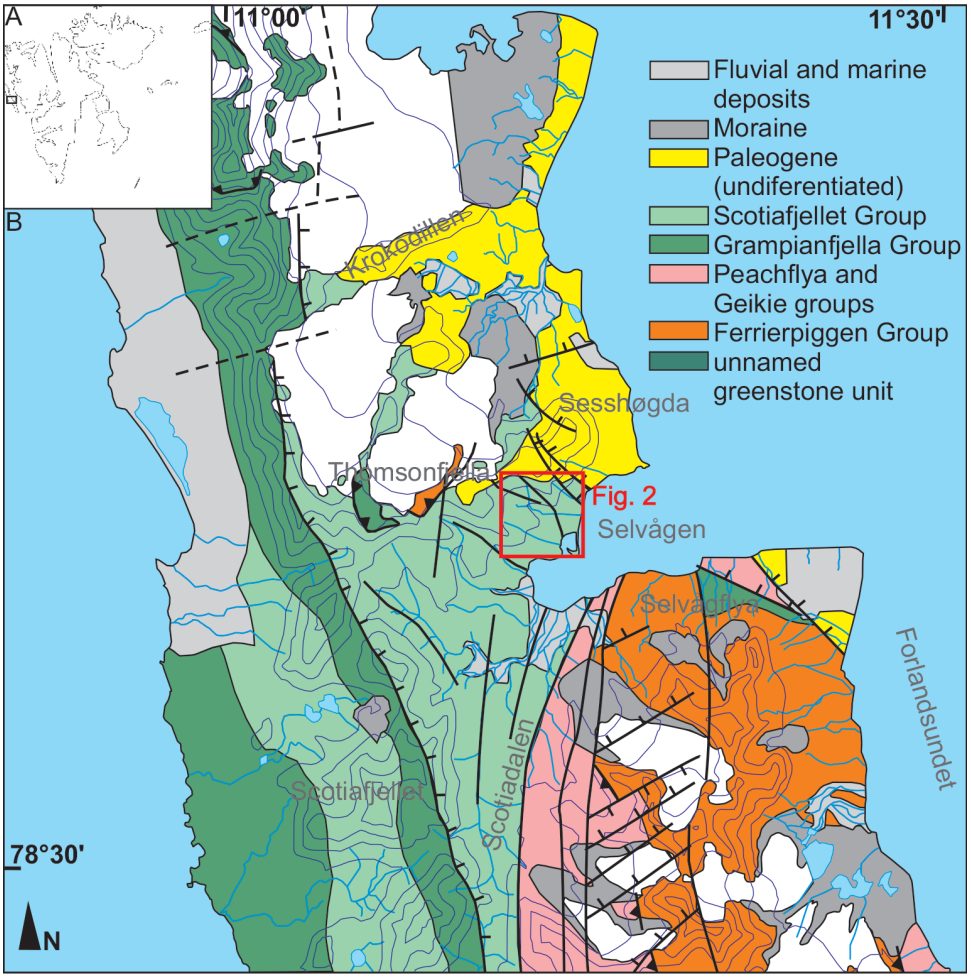

Figure 1. (A) Simplified map of Svalbard. Outlined box shows the location of Figure 1b; (B) Geological map of central Prins Karls Foreland (after Dallmann, 2015). Fig. 2a marked with red rectangle.

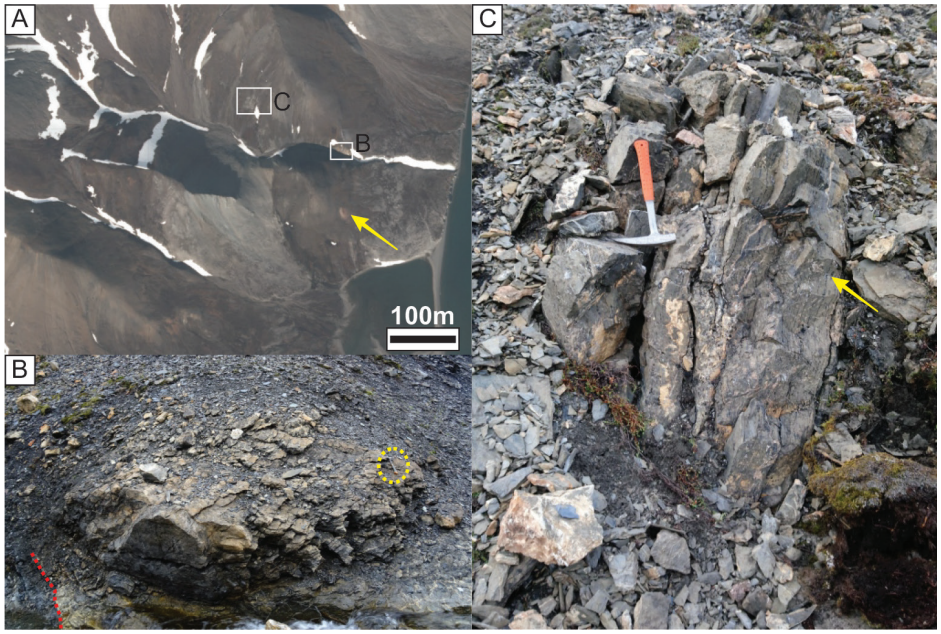

Figure 2. (A) Satellite image of the sampling area. Example of carbonate vein rich in siderite marked with yellow arrow. (toposvalbard.no) (B) Outcrop of magnesite in contact with surrounding black marbles and phyllites marked with red dotted line. (C) Close up image of the magnesite outcrop with visible bands of black metachert (marked by arrow). Note multiple dolomite veins crosscutting the vertical foliation within magnesite.

GPS coordinates: 78.5527188°N 11.2331401°E). The rock contains characteristic black, discontinuous, parallel bands of cherts. To date, massive metacarbonates with chert nodules were sampled only in the northern part of Scotiafjellet Group and studied only in the context of microfossils (Knoll & Ohta, 1988). Paleontological constrains suggest a late Neoproterozoic age of the studied metacarbonate.

2.2. Methods

Samples were collected from an outcrop during the 2018 Geological Expedition to Svalbard, organized by the Department of Mineralogy, Petrography, and Geochemistry at AGH University of Kraków. Petrographic analyses of thin sections were conducted using optical microscopy (under polarized light, Carl Zeiss Primotech), scanning electron microscopy coupled with energy-dispersive spectrometry (SEM/EDS; FEI Quanta 200 FEG, operated in low-vacuum mode without sample coating). Mineral composition was determined using powder X-ray diffraction (XRD, Rigaku Miniflex 600, CuK_{α} monochromatic radiation, step size 0.05° 2θ). Raman spectroscopy was performed using a DXR Raman Microscope (Thermo Fisher Scientific) equipped with a confocal Olympus BX-40 reflected light microscope and a 10 W, 514.5 nm laser, with spectra collected over the range of 100–3585 cm^{-1}. Spectral data were processed using *Omnic* (Thermo Fisher Scientific) and *PeakFit 4.12* software (Systat Software) packages. Mineral abbreviations in this article are according to Whitney & Evans (2010).

3. Results

3.1. Petrography

The outcrops of magnesite rock that belongs to Taylorfjellet Formation of the Scotiafjellet group are dispersed along the unnamed hill on the northern side of Selvågen (Fig. 2A). The thickness of the metacarbonates can be estimated to several tens of meters. The rocks are poorly exposed but locally the contact with surrounding calcite dominated black marbles and phyllites can be observed as conformable (Fig. 2B). Surrounding lithologies do not contain chert bands. The cryptocrystalline metacarbonate exhibits distinctive black, discontinuous, and parallel chert bands as well as pale orange dolomite veins (Fig. 2C). The rock displays well-developed foliation that is parallel to the chert banding, with foliation locally deflected around the margins of chert nodules (Fig. 3A). This deformation likely reflects compaction of the carbonate sediment during diagenesis and early stages of metamorphism. Contacts between the chert bands and the carbonate matrix range from sharp to gradational.

The rock is composed predominantly of magnesite and quartz, with minor dolomite, scattered pyrite grains, and occasional plagioclase and mica (Figs 3B and 4). The fine-grained carbonate matrix is cryptocrystalline and largely structureless aside from the foliation, with individual crystals typically a few micrometers in size (Figs 4A, B). Locally, larger crystals of magnesite and dolomite occur within the matrix. The crystal size, subhedral forms, and sharp grain boundaries collectively suggest that the carbonates recrystallized from the original sedimentary precursor to their present metamorphic texture.

Chert bands within the cryptocrystalline metacarbonate are typically several millimeters thick, while chert nodules range from several hundred micrometers to a few centimeters in diameter (Figs 4A–C). Chert occurs as both bands and nodules, though no significant compositional or textural differences have been observed between these two morphologies. The alignment of the nodules parallel to the general banding suggests they may represent boudins. However, the relationship between the chert structures

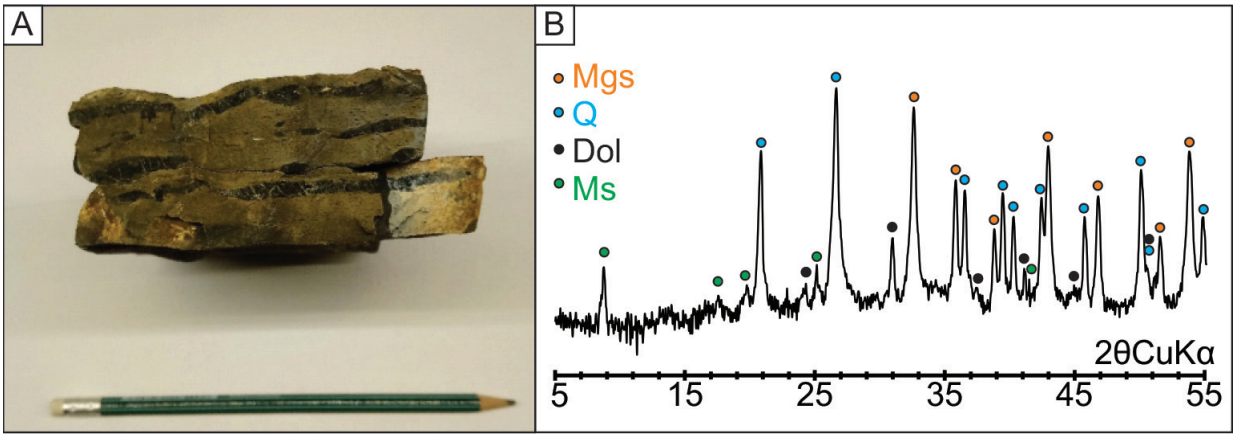

Figure 3. (A) Photograph of a sample of the metacarbonate with cherts. Cherts are preserved as horizontal black discontinuous bands and smaller nodules within microcrystalline metacarbonate matrix (B) Mineral composition of the metacarbonate rock based on the XRD pattern.

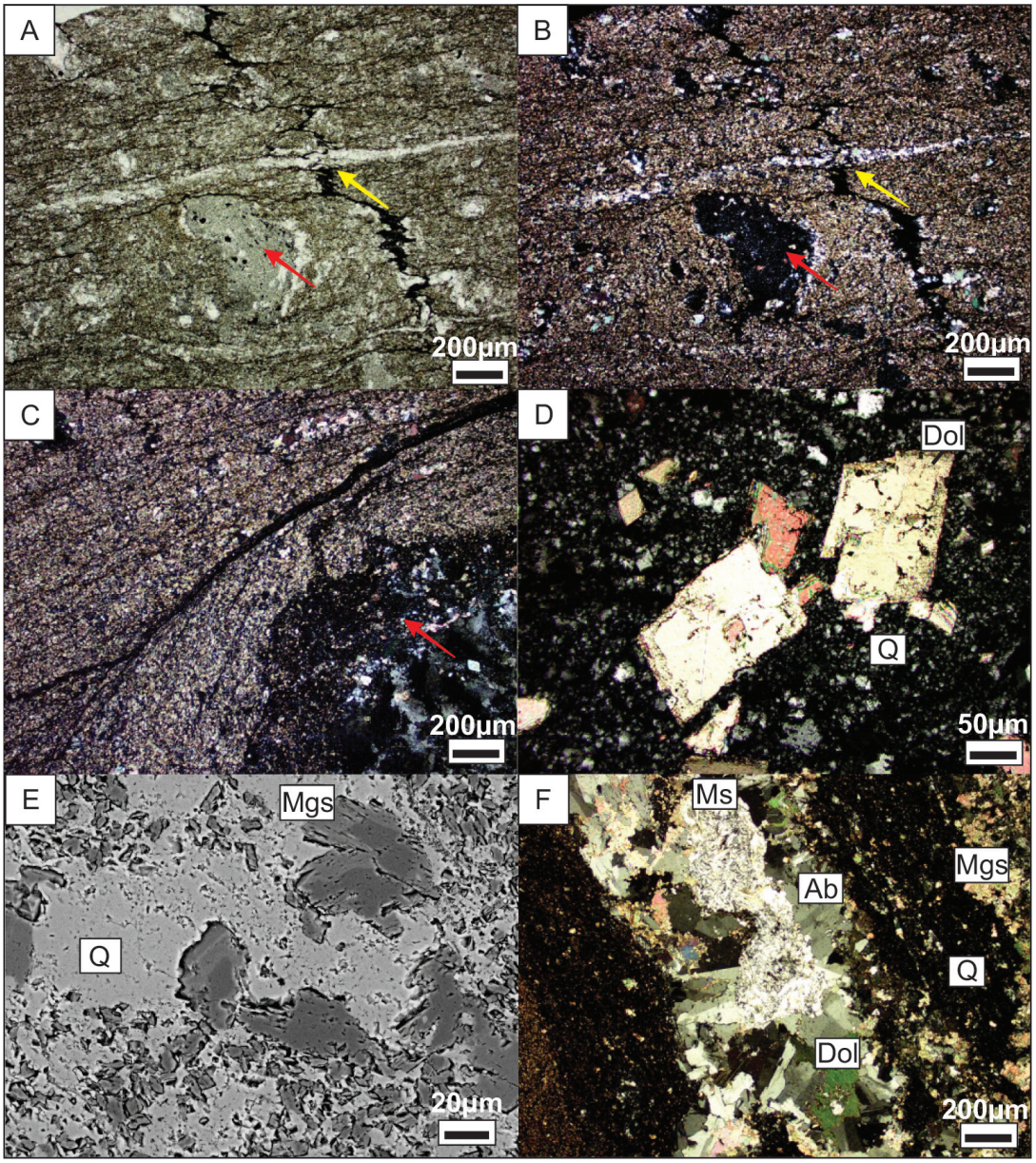

Figure 4. (A, B) Microphotographs of laminated magnesite rock around a small chert nodule in the centre (red arrow). A stylolite (yellow arrow) oblique to foliation and crosscut by a dolomitic vein is apparent (optical microscopy, A—1N, B—NX). (C) Foliation deflected around chert nodule marked with red arrow (D). Euhedral dolomite crystals embedded in finely crystalline silica of the chert (optical microscopy, NX). (E) Subhedral, zoned magnesites embedded in chert quartz matrix (SEM/BSE image). (F) First generation of dolomitic veins with albite and muscovite present.

and the magnesite host rock does not provide conclusive evidence as to whether the banding reflects primary sedimentary layering or the development of metamorphic foliation. Further investigation focusing on sedimentary structures is warranted.

The cherts are predominantly structureless, composed of fine-grained quartz with disseminated euhedral dolomite crystals within a siliceous matrix (Fig. 4D). Quartz grains typically measure a few micrometers, with coarser grains concentrated near chert margins. Grain contacts are sharp and locally sutured, indicating recrystallization under pressure. Euhedral dolomite crystals reach approximately 100 µm in size and their textural relationship with quartz suggests formation through neomorphic processes.

Scanning electron microscopy reveals zoning in magnesite crystals (Fig. 4E), characterized by pure magnesite core and iron-enriched rims (Table 1). This zoning is present in both larger recrystallized grains and finer matrix crystals, implying an evolution of the source fluid chemistry. The magnesite cores likely crystallized during early diagenetic magnesitization, whereas the Fe-enriched rims formed later from metamorphic fluids during deeper burial.

Chert bodies contain abundant carbonaceous material, although its preservation is compromised by low-grade metamorphism. Despite degradation, several putative biogenic structures can be identified. Most carbonaceous remnants appear as detrital agglomerates with subtle color variation relative to the surrounding chert matrix (Fig. 5A). Some of these aggregates contain microstructures resembling primitive organisms, including dispersed cyanobacterial cells and spherical clusters, possibly representing microbial colonies, infilled with framboidal pyrite (Fig. 5B). Due to poor preservation, definitive identification is challenging; however, these features are broadly comparable to microfossils described from the northern Scotiafjellet Group (Knoll, 1992), which appear to have experienced less alteration. The cherts of this unit thus remain promising targets for future paleobiological investigations.

Table 1. Representative elemental composition of magnesite rim and core (semi-quantitative SEM/EDS analysis normalized to 100%).

COMPONENT	CORE		RIM	
	wt%	mol%	wt%	mol%
CO_2	52	51	52	51
MgO	47	49	44	48
Fe_2O_3	1	0.2	4	1

Stylolites are present within the metacarbonate, oriented obliquely to foliation and commonly folded around larger, partially dissolved quartz grains. No dissolution features were observed in magnesite crystals. Locally, secondary carbonate veins crosscut stylolites, indicating vein formation postdates chemical compaction. The oblique orientation of stylolites relative to foliation suggests deformation postdating diagenesis. Quartz appears to have resisted dissolution, rendering the stylolites inactive in quartz-rich zones. The absence of dissolution features at magnesite contacts may imply either complete dissolution of earlier magnesite during stylolitization or subsequent recrystallization of magnesite after stylolite formation.

The magnesite–dolomite metacarbonate hosts multiple generations of carbonate veins (Fig. 6A), predominantly composed of authigenic dolomite crystals ranging from several micrometers to over one millimeter in size. The first-generation veins consist of dolomite, with subordinate feldspar and muscovite mica occurring as fine-grained aggregates. Rare magnesite crystals exceeding 1 mm are also present. SEM/Backscattered electron (BSE) imaging reveals magnesite grains rimmed by reaction zones, characterized by elevated iron concentrations in adjacent dolomite crystals (Fig. 6B). A second generation of dolomite veins crosscuts the earlier assemblage and is composed of finer crystals (up to several micrometers). Contacts between these younger veins and the host rock vary from sharp to gradational. In places, vein minerals from both generations are disseminated into the surrounding matrix. Sporadic feldspar grains exceeding 200 µm with characteristic albite twinning were identified (Fig. 4F). Raman spectroscopy and SEM/EDS analysis confirm the composition of these grains as pure albite.

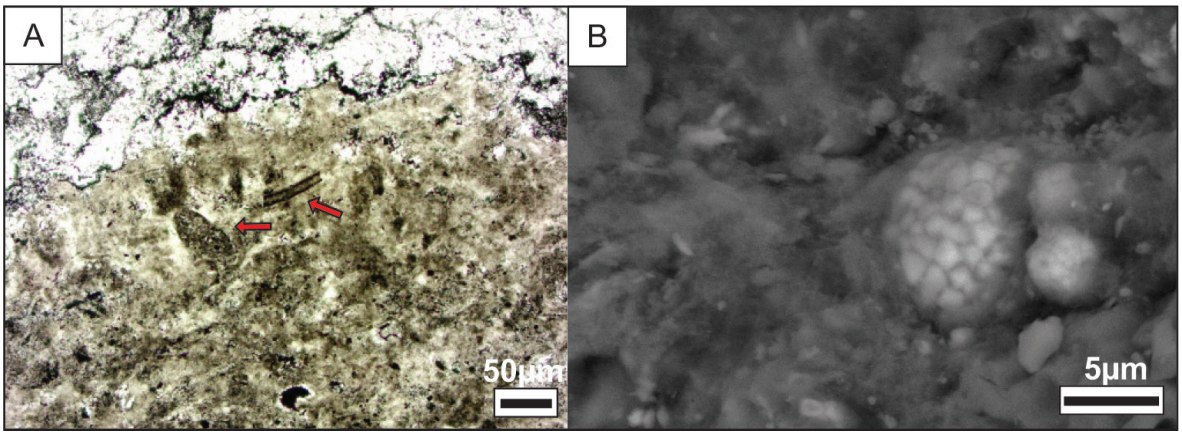

Figure 5. (A) Aggregates of detritus with biogenic structures (red arrows) (optical microscopy, 1N). (B) Framboidal pyrite embedded in chert. (SEM/BSE image).

3.2. *Raman geothermometry*

The metamorphic temperature was estimated using the Raman spectroscopy-based geothermometer of Kouketsu et al. (2014), which relies on the deconvolution of Raman spectra of carbonaceous matter. The spectrum was acquired from carbonaceous inclusions within quartz grains to minimize potential artefacts associated with surface polishing. Spectral processing was performed with PeakFit 4.12 software, employing Lorentzian functions for peak fitting. The spectral decomposition followed the fitting 'F' protocol recommended by Kouketsu et al. (2014), with the positions of the D4 and G bands fixed at 1245 cm^{-1} and 1593 cm^{-1}, respectively.

The Raman spectrum of carbonaceous matter reveals two broad bands centered near 1349 cm^{-1} and 1603 cm^{-1} (Fig. 7), corresponding to the D1 and G bands of disordered graphite (Beyssac et al., 2002; Kouketsu et al., 2014). The broad feature near 1603 cm^{-1} is interpreted as an overlap of the G and D2 bands and is hereafter referred to as G_L (G-Low). An elevated background in the 1100–1200 cm^{-1} range reflects the presence of the broad D4 band. A 1615 cm^{-1} is assigned to D2 (which typically appears around 1620 cm^{-1}). The D3 band is identified at ~1531 cm^{-1}. The presence of both D4 and G_L bands suggests that the carbonaceous matter is of low metamorphic grade. Following the fitting 'F' procedure, for which the intensity ratio G_L/D1 is below 1.5. Peaks were extracted using Lorentzian functions, while maintaining fixed positions for the D4 and G bands. The results of spectral deconvolution are summarized in Table 2 and Figure 7.

Table 2. Carbonaceous matter Raman bands positions after decomposition (FWHM).

BAND	CENTRE	INTENSITY	FWHM
D4	1244.6	18	381
D1	1349.4	142	80
D3	1531.2	19	144
G	1593.0	73	44
D2	1615.2	63	33

FWHM, full width at half maximum.

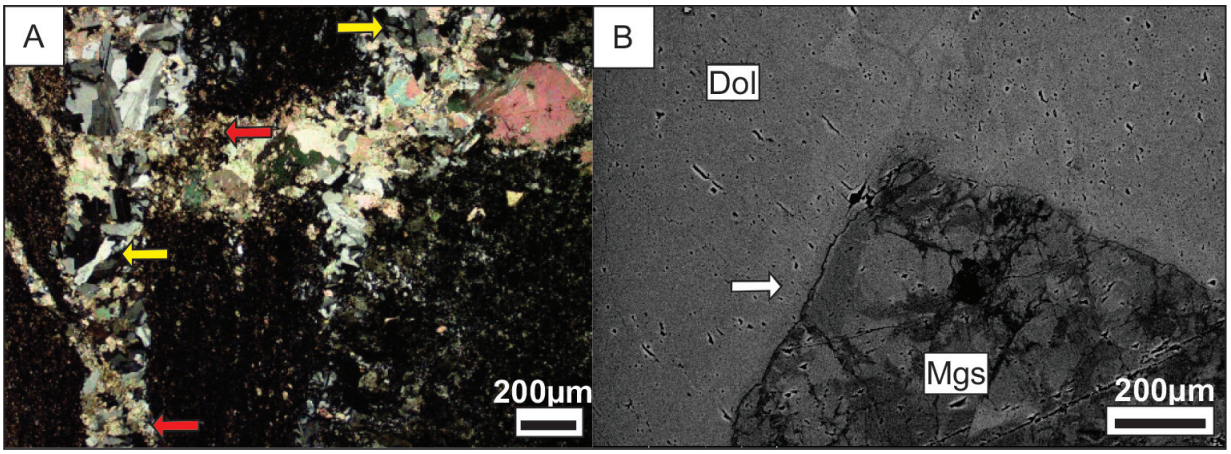

Figure 6. (A) Second generation dolomite veins (red arrows) crosscutting the first generation albite veins (yellow arrows; optical microscopy, NX). (B) BSE image of the reaction rim around the magnesite grain manifested by elevated Fe content in dolomite (white arrow).

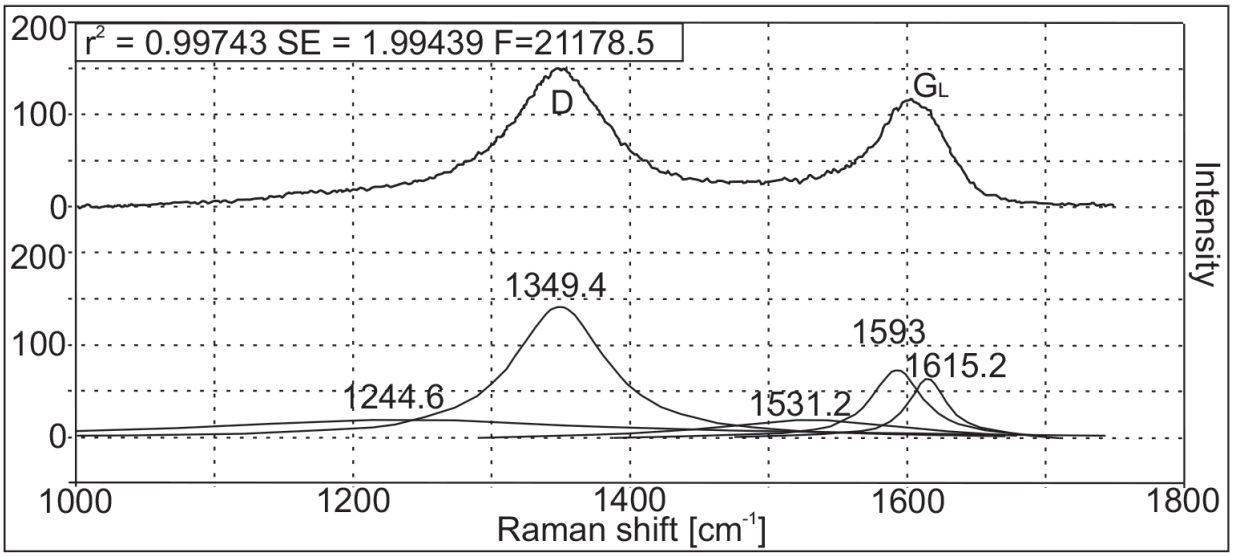

Figure 7. Raman spectrum of carbonaceous matter (top) and its deconvolution (bottom); R^2—coefficient of determination, SE, *F*—area. SE, standard error.

Temperature estimates were calculated using two empirical formulas from Kouketsu et al. (2014):

$$T_1\ (^{o}C) = -2.15(FWHM\_D1) + 478 \quad (1)$$

$$T_2\ (^{o}C) = -6.78(FWHM\_D2) + 535 \quad (2)$$

where FWHM means full width at half maximum. The resulting temperatures $T_1 = 305 \pm 30°C$ and $T_2 = 309 \pm 50°C$ are identical within analytical uncertainty and consistent with the temperature range inferred from the formation of albite in the rock (Spötl et al., 1999). Attempts to apply additional geothermometers were unsuccessful. Application of the Beyssac et al. (2002) geothermometer based on D1, G, and D2 bands in Raman spectra proved inconclusive owing to the ambiguous resolution of the G and D2 bands (data not shown). The absence of graphite reflections in XRD patterns of cherts precluded the use of the Shengelia et al. (1977) method, likely due to the low crystallinity of the carbonaceous matter and potential peak overlap with quartz.

4. Discussion

4.1. Classification of magnesite deposit

The magnesites from PKF are characterized by paragenesis containing mainly magnesite and quartz with minor dolomite, pyrite, white mica and organic matter. Their association with fossiliferous cherts suggests that a carbonaceous protolith was affected by metasomatic changes to produce magnesite. Two sets of dolomitic veins shed more light on this process. The first generation of veins with dolomite, magnesite albite and muscovite notably cut only the chert layers and boudinaged fragments, but do not cut the magnesites (Figs 4A, B). When reaching the boundary of two lithologies they become finer-grained and follow the edge of the chert. It is in line with the different behaviour of the two protoliths i.e. magnesite rock behaves plastically while cherts remain brittle. This contrast in rheological behaviour resulted most likely in the opening of fractures in chert layers that allowed the infiltration of the Mg-rich fluid into primary carbonates.

The secondary carbonate veins built of dolomite cut the cherts, magnesites and primary veins (Fig. 7). Some of them also follow the foliation planes in magnesites which suggest that they were formed already in post-kinematic stage, likely during the uplifting of the whole complex back to the brittle regime depths. Reaction halos in the primary veins suggest that magnesite was replaced by dolomite which was accompanied by increase of the iron content in dolomite. Substantial amounts of Ca^{2+} released during magnesite formation may later result in its redolomilitization (Aharon, 1988). The metasomatic replacement of dolomite is controlled by temperature where an increase in temperature results in magnesitization whereas a decrease in temperature may lead to redolomitization (Krupenin et al., 2013). Therefore, observed interaction suggests the redolomization that was likely coeval with the introduction of the secondary veins.

The rheological behaviour of the magnesite rock suggests that the process occurred in the metamorphic conditions of the greenschist facies. This is corroborated by geothermometry estimates based on Raman spectra of carbonaceous matter (Kouketsu et al., 2014) that yielded the results of 260–360°C, well in the lower greenschist facies. Composition of the primary carbonate veins also supports these metamorphic conditions. The occurrences of authigenic albite in carbonate rocks are related to deep-burial environments, i.e. very low-grade metamorphic to low-grade metamorphic rather than diagenetic. Formation of albite seems to be the result of the interaction between carbonates and NaCl brines in pore solution at temperatures corresponding to either high-grade diagenesis (~150–200°C) or low greenschist facies (~300–350°C) (Spötl et al., 1999).

The order of events as well as the observed structures are remarkably similar to the development of the Veisch-type magnesite in their type locality (Wölfler et al., 2015). There, a precursor coarse dolomite rock is locally metasomatized to coarser magnesite crystals which is followed by late-stage metasomatic reaction of dolomite into fine-grained magnesites. The whole process is similarly followed by development of the secondary dolomite-quartz veins (Wölfler et al., 2015). The conformable contact with surrounding phyllites and marbles suggest that the magnesite occurrence can be tentatively classified as stratabound. Sedimentary sequence of a marine shelf, structural and compositional characteristics, as well as an elevated iron content imply that the forming of the magnesite rock can be explained by Veitsch-type model (Pohl, 1989).

4.2. Magnesite formation and its regional significance

The magnesite formation in PKF was a result of metasomatism of the primary carbonate in presence of Mg rich fluid. The origin of the fluid cannot be determined without proper oxygen isotope studies, however observed structures would suggest that in the lower greenschist metamorphic conditions it could have originated in the deeper part of the crust. To date the timing of the metamorphism is assumed to be Caledonian and related to the formation of the westward translated nappe stack (Manby, 1986). Discontinuities related to the nappe stacking are frequently associated with voluminous carbonate veining (e.g. Fig. 2A), which is likely related to the deeper-seated mobilisation of carbonate fluid.

The only other occurrence of magnesite bodies in Svalbard in Oscar II Land is related to metasomatism of the suture marking ultramafic rocks (Ohta et al., 1995). The age of the late Caledonian structures in Oscar II Land is considered coeval to the ones developed in PKF, however the vergence of the structures is opposite. Recent studies in the Mullerneset area showed that between the PKF and Oscar II Land the zone of intensive shearing was documented and possibly incorporates the suture related Vestgötabreen Complex (Ziemniak et al., 2022). The origin of the Mg rich fluid that resulted

in formation of the magnesite in PKF might be therefore related to mobilisation of the Mg from lithologies Lower Unit of Vestgötabreen Complex involved in the late Caledonian sinistral shearing.

Similar ultramafic origin of the Mg rich fluid was proposed for the formation of the Hirsizdere sedimentary magnesite deposit in Turkey (Zedef et al., 2000) and Kamado deposit in China (Yu et al., 2024). Nevertheless this deposits formed in relatively lower temperatures then the magnesite from PKF. For higher temperatures of formation in Veitsch type deposit a metamorphic fluid is invoked as a main cause of magnesitization (e.g. Schroll, 2002). Some of the authors suggest that the fluid may have its origin in ultramafic rocks (e.g. Kiesl et al., 1990), however REE patterns do not match seawater or ultramafic protolith of the fluid (Schroll, 2002).

Nevertheless, more detailed studies, including more detailed field investigation and isotopic analysis, are required to understand the formation process of the magnesites from PKF.

Acknowledgments

MM was supported by AGH research funds No 16.16.140.315. We thank Aratz Beranoaguirre and an anonymous reviewer for constructive reviews. We also thank Aratz Beranoaguirre and Iwona Klonowska for editorial handling.

References

Aharon, P. (1988). A stable-isotope study of magnesites from the Rum Jungle Uranium Field, Australia: Implications for the origin of strata-bound massive magnesites. *Chemical Geology, 69*(1–2), 127–145. https://doi.org/10.1016/0009-2541(88)90164-7

Bernard-Griffiths, J., Peucat, J. J., & Ohta, Y. (1993). Age and nature of protoliths in the Caledonian blueschist-eclogite complex of Western Spitsbergen: A combined approach using U U-Pb, Sm-Nd and REE whole-rock systems. *Lithos, 30*(1), 81–90. https://doi.org/10.1016/0024-4937(93)90007-Y

Beyssac, O., Goffé, B., Chopin, C., & Rouzaud, J. N. (2002). Raman spectra of carbonaceous material in metasediments: A new geothermometer. *Journal of Metamorphic Geology, 20*(9), 859–871. https://doi.org/10.1046/j.1525-1314.2002.00408.x

Dallmann, W. K. (2015). *Geoscience atlas of Svalbard*. Norsk Polarinstitutt.

Gee, D. G., & Teben'kov, A. M. (2004). Svalbard: A fragment of the Laurentian margin. *Geological Society, London, Memoirs, 30*(1), 191–206. https://doi.org/10.1144/GSL.MEM.2004.030.01.16

Hjelle, A., Ohta, Y., & Winsnes, S. (1979). Hecla Hoek rocks of Oscar II Land and Prins Karls Forland, Svalbard. *Norsk Polarinstitut Skrifter, 167*, 145–169.

Kiesl, W., Koeberl, C., & Körner, W. (1990). Geochemistry of magnesites and dolomites at the Oberdorf/Laming (Austria) deposit and implications for their origin. *Geologische Rundschau, 79*(2), 327–335. https://doi.org/10.1007/BF01830629

Knoll, A. H., & Ohta, Y. (1988). Microfossils in metasediments from Prins Karls Forland, Western Svalbard. *Polar Research, 6*(1), 59–67. https://doi.org/10.1111/j.1751-8369.1988.tb00581.x

Knoll, A. H. (1992). Vendian microfossils in metasedimentary cherts of the Scotia Group, Prins Karls Forland, Svalbard. *Palaeontology, 35*(4), 751–774.

Kośmińska, K., Spear, F. S., Majka, J., Faehnrich, K., Manecki, M., Piepjohn, K., & Dallmann, W. K. (2020). Deciphering late Devonian–early Carboniferous P–T–t path of mylonitized garnet-mica schists from Prins Karls Forland, Svalbard. *Journal of Metamorphic Geology, 38*(5), 471–493. https://doi.org/10.1111/jmg.12529

Kouketsu, Y., Mizukami, T., Mori, H., Endo, S., Aoya, M., Hara, H., Nakamura, D., & Wallis, S. (2014). A new approach to develop the Raman carbonaceous material geothermometer for low-grade metamorphism using peak width. *Island Arc, 23*(1), 33–50. https://doi.org/10.1111/iar.12057

Krupenin, M. T., Kol'tsov, A. B., & Maslov, A. V. (2013, October). Physicochemical model of the formation of Satka sparry magnesite deposits. *Doklady Earth Sciences, 452*(2), 1020–1022. https://doi.org/10.1134/S1028334X13100048

Majka, J., & Kośmińska, K. (2017). Magmatic and metamorphic events recorded within the Southwestern Basement Province of Svalbard. *Arktos, 3*, 1–7. https://doi.org/10.1007/s41063-017-0034-7

Manby, G. M. (1986). Mid-Palaeozoic metamorphism and polyphase deformation of the Forland Complex, Svalbard. *Geological Magazine, 123*(6), 651–663. https://doi.org/10.1017/S001675680002416X

Ohta, Y., Krasil'Šikov, A. A., Lepvrier, C., & Teben'kov, A. M. (1995). Northern continuation of Caledonian high-pressure metamorphic rocks in central-western Spitsbergen. *Polar Research, 14*(3), 303–316. https://doi.org/10.1111/j.1751-8369.1995.tb00717.x

Pohl, W. (1989). Comparative geology of magnesite deposits and occurrences. In *Monograph series on mineral deposits.* Möller, P. (Ed) (Vol. 28, pp. 1–13). Gebrüder Borntraeger.

Scheller, E. L., Swindle, C., Grotzinger, J., Barnhart, H., Bhattacharjee, S., Ehlmann, B. L., Farley, K., Fischer, W. W., Greenberger, R., Ingalls, M., Martin, P. E., Osorio-Rodriguez, D., & Smith, B. P. (2021). Formation of magnesium carbonates on Earth and implications for Mars. *Journal of Geophysical Research: Planets, 126*(7), e2021JE006828. https://doi.org/10.1029/2021JE006828

Schneider, D. A., Faehnrich, K., Majka, J., & Manecki, M. (2019). $^{40}Ar/^{39}Ar$ geochronologic evidence of eurekan deformation within the West Spitsbergen Fold and Thrust Belt. In: Piepjohn, K., Strauss, JV., Reinhardt, L., and McClelland, W.C. (Ed) Circum-arctic structural events: Tectonic evolution of the arctic margins and trans-arctic links with adjacent orogens. *Geological Society of America, 541*, 1–16. https://doi.org/10.1130/2018.2541(08)

Schroll, E. (2002). Genesis of magnesite deposits in the view of isotope geochemistry. *Boletim paranaense de geociencias, 50*, 59–68. https://doi.org/10.5380/geo.v50i0.4158

Shengelia, D. M., Akvlediani, R. A., & Ketskhoveli, D. N. (1977). Graphite thermometer. *Doklady Akademii Nauk SSSR, 235*(6), 1407–1409.

Spötl, C., Longstaffe, F. J., Ramseyer, K., & Rüdinger, B. (1999). Authigenic albite in carbonate rocks – A tracer for deep-burial brine migration? *Sedimentology, 46*(4), 649–666. https://doi.org/10.1046/j.1365-3091.1999.00237.x

Tyrrell, G. W. (1924). The geology of Prince Charles Foreland, Spitsbergen. *Earth and Environmental Science Transactions of the Royal Society of Edinburgh, 53*(2), 443–478. https://doi.org/10.1017/S0080456800004117

Wala, V. T., Ziemniak, G., Majka, J., Faehnrich, K., McClelland, W. C., Meyer, E. E., Manecki, M., Bazarnik, J., & Strauss, J. V. (2021). Neoproterozoic stratigraphy of the Southwestern Basement Province, Svalbard (Norway): Constraints on the Proterozoic-Paleozoic evolution of the North Atlantic-Arctic Caledonides. *Precambrian Research, 358*, 106138. https://doi.org/10.1016/j.precamres.2021.106138

Wölfler, A., Prochaska, W., & Fritz, H. (2015). Shear zone related talc mineralizations in the Veitsch Nappe of the Eastern Greywacke Zone (Eastern Alps, Austria). *Austrian Journal of Earth Sciences, 108*(1), 50–72. https://doi/10.17738/ajes.2015.0004

Yu, X., Hu, G., Chen, Y., Xu, Y., Chen, H., Wang, D., Huang, F., You, S., Liu, H., He, L., & Li, Y. (2024). Genesis of the large-scale kamado magnesite deposit on the Tibetan Plateau. *Minerals, 14*(1), 45. https://doi.org/10.3390/min14010045

Zedef, V., Russell, M. J., Fallick, A. E., & Hall, A. J. (2000). Genesis of vein stockwork and sedimentary magnesite and hydromagnesite deposits in the ultramafic terranes of southwestern Turkey: A stable isotope study. *Economic Geology, 95*(2), 429–445. https://doi.org/10.2113/gsecongeo.95.2.429

Ziemniak, G., Manecki, M., Jeanneret, P., Walczak, K., & Kośmińska, K. (2022). Early Devonian sinistral shearing recorded by retrograde monazite-(Ce) in Oscar II Land, Svalbard. *Mineralogia, 53*(1), 82–108. https://doi.org/10.2478/mipo-2022-0007

Received: 26 Sep 2025
Accepted: 29 Nov 2025
Handling Editor: Aratz Beranoaguirre